

# Convergence of a three-dimensional quantum lattice Boltzmann scheme towards solutions of the Dirac equation

BY DENIS LAPITSKI AND PAUL J. DELLAR

*OCIAM, Mathematical Institute, 24-29 St Giles', Oxford OX1 3LB, UK*

We investigate the convergence properties of a three-dimensional quantum lattice Boltzmann scheme for the Dirac equation. These schemes were constructed as discretisations of the Dirac equation based on operator splitting, but their output has previously only been compared against solutions of the Schrödinger equation. The Schrödinger equation arises as the non-relativistic limit of the Dirac equation, describing solutions that vary slowly compared to the Compton frequency. We demonstrate first-order convergence towards solutions of the Dirac equation obtained by an independent numerical method based on fast Fourier transforms and matrix exponentiation.

**Keywords:** quantum lattice Boltzmann, Dirac equation, Schrödinger equation

## 1. Introduction

The lattice Boltzmann approach to computational hydrodynamics relies on the Navier–Stokes equations describing slowly varying solutions of the Boltzmann equation. The same property holds when the continuous velocity space of standard kinetic theory is truncated to obtain a discrete Boltzmann equation, which we write as (Chen & Doolen, 1998; Succi, 2001; Benzi *et al.*, 1992)

$$(\partial_t + \boldsymbol{\xi}_i \cdot \nabla) f_i = \sum_{j=0}^n \Omega_{ij} (f_j - f_j^{(0)}), \quad (1.1)$$

for  $i = 0, \dots, n$ . The distribution functions  $f_i$  propagate in the directions given by the discrete velocities  $\boldsymbol{\xi}_i$ , and relax towards their equilibrium values  $f_i^{(0)}$  through the action of the collision matrix  $\Omega_{ij}$ .

The quantum lattice Boltzmann (QLB) schemes introduced by Succi & Benzi (1993) exploit the structural similarities between the discrete Boltzmann equation and the Dirac equation of quantum electrodynamics (Berestetskii *et al.*, 1982). Both are linear, symmetric hyperbolic systems with algebraic source terms, so numerical algorithms for the Dirac equation may be obtained by applying the same techniques that lead from the discrete Boltzmann equation to lattice Boltzmann schemes for hydrodynamics (see Succi, 1996, 2001; Palpacelli & Succi, 2007). QLB schemes may also be interpreted as cellular automata that evolve probability amplitudes (qbits) rather than bits (Bialynicki-Birula, 1994; Meyer, 1996). Palpacelli & Succi (2008) have surveyed recent applications of QLB schemes to simulate the

*Submitted 13 October 2010, accepted 21 January 2011.*

Schrödinger equation of non-relativistic quantum mechanics. The Schrödinger equation describes slowly varying solutions of the Dirac equation, in close analogy with the derivation of the Navier–Stokes equations as describing slowly varying solutions of the Boltzmann equation. However, attention has not previously been paid to the properties of QLB schemes for computing solutions to the Dirac equation itself.

## 2. The Dirac equation

The Dirac equation offers a quantum mechanical description of an electron that is compatible with special relativity (Berestetskii *et al.*, 1982). Its standard form is

$$(\partial_t + c\boldsymbol{\alpha} \cdot \nabla) \psi = -i\omega_c \beta \psi + ig\psi, \quad (2.1)$$

where  $c$  is the light speed,  $\hbar$  is the reduced Planck's constant, and  $\omega_c = mc^2/\hbar$  is the Compton frequency for a particle of mass  $m$ . The wavefunction  $\psi$  is a column vector with 4 components,  $\beta$  is a  $4 \times 4$  matrix, and  $\boldsymbol{\alpha} = (\alpha^x, \alpha^y, \alpha^z)$  is a collection of three  $4 \times 4$  matrices, so that  $\boldsymbol{\alpha} \cdot \nabla = \alpha^x \partial_x + \alpha^y \partial_y + \alpha^z \partial_z$ . The last term couples the wavefunction to an applied scalar potential  $V$  via the coefficient  $g = qV/\hbar$ , where  $q > 0$  is the modulus of the charge on an electron. This sign convention was used in previous QLB schemes, but it differs from that in Berestetskii *et al.* (1982).

The  $4 \times 4$  matrices  $\alpha^i$  and  $\beta$  may be written in block form as

$$\alpha^i = \begin{pmatrix} 0 & \sigma^i \\ \sigma^i & 0 \end{pmatrix}, \quad \beta = \begin{pmatrix} 1 & 0 \\ 0 & -1 \end{pmatrix}, \quad (2.2)$$

where  $1$  is the  $2 \times 2$  identity matrix. The off-diagonal blocks are Pauli spin matrices,

$$\sigma^x = \begin{pmatrix} 0 & 1 \\ 1 & 0 \end{pmatrix}, \quad \sigma^y = \begin{pmatrix} 0 & -i \\ i & 0 \end{pmatrix}, \quad \sigma^z = \begin{pmatrix} 1 & 0 \\ 0 & -1 \end{pmatrix}, \quad (2.3)$$

that satisfy the well-known commutation relations (Berestetskii *et al.*, 1982)

$$\sigma^i \sigma^j - \sigma^j \sigma^i = 2i \epsilon_{ijk} \sigma^k, \quad (2.4)$$

where  $\epsilon_{ijk}$  is the alternating Levi-Civita tensor. The  $\alpha$  matrices are all Hermitian, and hence diagonalisable, but the commutators of their non-zero blocks do not vanish. There is thus no basis in which the  $\alpha$  matrices are simultaneously diagonal.

Writing the wavefunction as  $\psi = (\phi_1^+, \phi_2^+, \phi_1^-, \phi_2^-)^\top$ , the  $\pm$  superscripts correspond to components with positive and negative energies. For a free particle these oscillate in proportion to  $\exp(\mp i\omega_c t)$  in the long-wave limit. The subscripts 1 and 2 label the two different spin states. To derive the Schrödinger equation one writes  $\psi = (\Phi_1^+, \Phi_2^+, \Phi_1^-, \Phi_2^-)^\top \exp(-i\omega_c t)$  to transform away the rest energy of the  $+$  states, assumes  $\partial_t \Phi_{1,2}^- \ll 2i\omega_c \Phi_{1,2}^-$ , equivalent to a non-relativistic limit, and substitutes the resulting adiabatic approximations for  $\Phi_{1,2}^-$  into the evolution equations for  $\Phi_{1,2}^+$ . Palpacelli & Succi (2008) give a derivation in this notation.

## 3. Quantum lattice Boltzmann schemes

The Dirac and discrete Boltzmann equations are both linear, symmetric, hyperbolic systems with algebraic source terms. However, the discrete Boltzmann equation is highly unusual among multi-dimensional hyperbolic systems in possessing one-dimensional characteristic curves of the form  $(\mathbf{x}, t) = (\mathbf{x}_0 + s\boldsymbol{\xi}_i, t_0 + s)$ ,

as parametrized by  $s$ . All one may expect in general is the existence of three-dimensional characteristic surfaces in four-dimensional  $(\mathbf{x}, t)$  space (Whitham, 1974).

The three  $\alpha$  matrices are not simultaneously diagonalisable, so the characteristics of the Dirac equation are indeed three-dimensional surfaces, the light cones of special relativity. Discontinuities in the initial conditions are confined to propagating along these surfaces, but there are no one-dimensional characteristic curves to integrate along. The approach that leads from the discrete Boltzmann equation to a lattice Boltzmann scheme (as in He *et al.*, 1998) thus cannot be employed.

Instead, multi-dimensional QLB schemes use operator splitting to approximate solutions to the three-dimensional Dirac equation using solutions of one-dimensional Dirac equations in which spatial dependences in the other two directions are temporarily neglected. For instance, neglecting dependence on  $y$  and  $z$  leads to

$$(\partial_t + c\alpha^x\partial_x)\psi = -\frac{1}{3}i\omega_c\beta\psi + \frac{1}{3}ig\psi. \quad (3.1)$$

The factor of  $1/3$  on the right hand side arises from dividing the algebraic terms into three equal parts, one associated with each spatial direction (Palpacelli & Succi, 2007). Each of these one-dimensional Dirac equations does have characteristic curves, since the  $\alpha$  matrices are Hermitian and thus diagonalisable. Equation (3.1) and its analogues in  $y$  and  $z$  may thus be evolved forward in time using the one-dimensional QLB algorithm described by Succi & Benzi (1993) and Succi (1996). It is convenient to choose units in which  $c = 1$  and  $\hbar = 1$ , so  $\Delta x = \Delta t$  and  $\omega_c = m$ .

Existing QLB schemes begin with the Majorana form of the Dirac equation (see Berestetskii *et al.*, 1982) but the same approach may be applied to the standard form (2.1) in which the algebraic terms are diagonal. The only disadvantage is that  $\alpha^y$  must be diagonalised by a complex matrix. The two approaches based on the Majorana and standard forms agree to within numerical round-off errors.

The three  $\alpha$  matrices in the standard form (2.1) may be diagonalised as

$$X^\dagger\alpha^xX = Y^\dagger\alpha^yY = Z^\dagger\alpha^zZ = \beta, \quad (3.2)$$

where  $\dagger$  denotes the Hermitian transpose, by the three unitary matrices

$$X = \frac{1}{\sqrt{2}} \begin{pmatrix} 1 & 0 & -1 & 0 \\ 0 & 1 & 0 & -1 \\ 0 & 1 & 0 & 1 \\ 1 & 0 & 1 & 0 \end{pmatrix}, Y = \frac{1}{\sqrt{2}} \begin{pmatrix} 0 & i & 0 & 1 \\ -i & 0 & i & 0 \\ -1 & 0 & -1 & 0 \\ 0 & -1 & 0 & -i \end{pmatrix}, Z = \frac{1}{\sqrt{2}} \begin{pmatrix} 1 & 0 & 0 & -1 \\ 0 & -1 & 1 & 0 \\ 1 & 0 & 0 & 1 \\ 0 & 1 & 1 & 0 \end{pmatrix}. \quad (3.3)$$

Thus the streaming step in  $x$  consists of multiplying  $\psi$  by  $X^\dagger$ , streaming  $\hat{\psi} = X^\dagger\psi$  in the  $x$  directions by  $\pm\Delta x$ , and finally multiplying  $\hat{\psi}$  by  $X$  to undo the transformation. The first QLB schemes suffered from numerical artifacts due to applying the  $X$  and  $X^\dagger$  matrices in the wrong order (see Dellar *et al.*, 2010). We also use operator splitting to separate the spatial derivatives from the algebraic terms, which are diagonal in the standard representation. The  $+$  components are

$$\partial_t\phi_{1,2}^+ = \frac{1}{3}i(g-m)\phi_{1,2}^+, \quad (3.4)$$

which we discretise using the Crank–Nicolson scheme to obtain

$$\frac{\phi_{1,2}^+(t+\Delta t) - \phi_{1,2}^+(t)}{\Delta t} = \frac{1}{6}i(g-m)(\phi_{1,2}^+(t+\Delta t) + \phi_{1,2}^+(t)). \quad (3.5)$$

The solution, and its analogue for  $\phi_{1,2}^-(t + \Delta t)$ , may be expressed in the manifestly unitary form

$$\phi_{1,2}^\pm(t + \Delta t) = \phi_{1,2}^\pm(t) \frac{1 + i\Delta t(g \mp m)/6}{1 - i\Delta t(g \mp m)/6}. \quad (3.6)$$

Writing the transformed post-collisional wavefunction as  $\hat{\psi} = (\hat{\phi}_1^+, \hat{\phi}_2^+, \hat{\phi}_1^-, \hat{\phi}_2^-)^\top$ , the QLB step for colliding and streaming in  $x$  may be written as

$$\psi(x, t + \Delta t) = X \begin{pmatrix} \hat{\phi}_{1,2}^+(x - \Delta t, t) \\ \hat{\phi}_{1,2}^-(x + \Delta t, t) \end{pmatrix}, \text{ where } \hat{\psi}(x, t) = X^\dagger \begin{pmatrix} \phi_{1,2}^+(x, t + \Delta t) \\ \phi_{1,2}^-(x, t + \Delta t) \end{pmatrix}. \quad (3.7)$$

The full QLB scheme combines this step with analogous collision and streaming steps in the  $y$  and  $z$  directions, as diagonalised by the  $Y$  and  $Z$  matrices.

#### 4. Free particle

We apply the QLB scheme described above to initial conditions in which the positive energy, spin-up component  $\phi_1^+$  is a spherically symmetric Gaussian wavepacket with spread  $\Delta_0$ , as in Palpacelli & Succi (2007),

$$\phi_1^+(x, y, z, t) = (2\pi\Delta_0^2)^{-3/4} \exp\left(-\frac{x^2 + y^2 + z^2}{4\Delta_0^2}\right). \quad (4.1)$$

The other three components  $\phi_2^+$  and  $\phi_{1,2}^-$  are initially set to zero. We study the dispersion of the wavepacket over time, as measured by the spread  $\Delta$  defined by

$$\Delta = \left(\int \frac{1}{3} |\mathbf{x}|^2 |\phi_1^+|^2 dV\right)^{1/2} / \left(\int |\phi_1^+|^2 dV\right)^{1/2}. \quad (4.2)$$

We approximate these integrals using the trapezium rule, which is exponentially accurate for equally spaced points in a domain with periodic boundary conditions.

According to the Schrödinger equation, the spread of this wavepacket grows as

$$\Delta_S(t) = \left(\Delta_0^2 + \frac{\hbar^2 t^2}{4m^2 \Delta_0^2}\right)^{1/2}. \quad (4.3)$$

Figure 1(a) shows the measured spread for a free particle with  $m = 0.35$  and  $\Delta_0 = 14$  in a cube with side length  $\ell = 200$  and periodic boundary conditions. All these quantities are expressed in natural units with  $c = 1$  and  $\hbar = 1$ . The cube was discretised using  $N^3$  points for  $N = 128, 256, 512, 1024$ . The computed spreads on the different grids all follow the general trend of the Schrödinger solution  $\Delta_S$ , but they are all subject to superimposed high frequency oscillations. Similar oscillations were seen in one-dimensional computations by Valdivieso & Muñoz (2009).

Figure 1(b) shows the differences between the measured spreads and the spread  $\Delta_S$  predicted by the Schrödinger equation. Also shown is the spread  $\Delta_D$  for a highly accurate numerical solution to the Dirac equation, computed as described in the next subsection. High frequency oscillations are also present in  $\Delta_D$ . These oscillations, at frequencies comparable to the Compton frequency, are an intrinsic feature of the Dirac equation as a relativistic theory that accounts for a particle's rest energy  $mc^2$  as well as kinetic energy due to its motion. Figure 2(a) shows second-order convergence of the measured spreads towards the spread  $\Delta_D$  of the reference solution. Further confirmation is given in figure 2(b), showing first-order convergence of the four fields  $\phi_{1,2}^\pm$  towards the reference solution in the  $L_2$  norm.

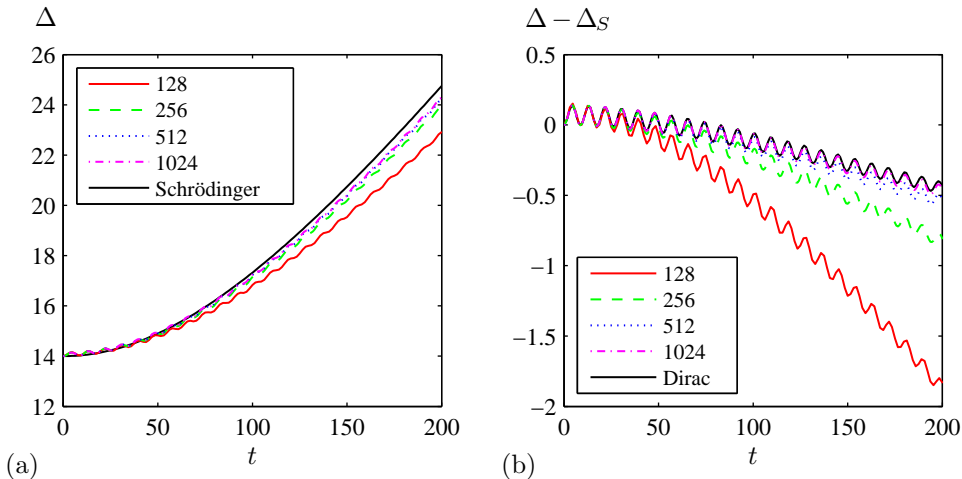


Figure 1. (Online version in colour.) (a) Evolution of the spread  $\Delta$  for different numbers of gridpoints. (b) Difference between the computed  $\Delta$  and the Schrödinger solution  $\Delta_S$ .

(a) *Reference solutions*

In the absence of a potential ( $g = 0$ ) the Dirac equation becomes a linear partial differential equation with constant coefficients. It is thus amenable to Fourier transform techniques. Substituting  $\psi(\mathbf{x}, t) = \tilde{\psi}(t) \exp(i\mathbf{k} \cdot \mathbf{x})$  into (2.1) leads to

$$i\partial_t \tilde{\psi} = \mathbf{H}_{\mathbf{k}} \tilde{\psi}, \quad (4.4)$$

with the  $4 \times 4$  matrix Hamiltonian  $\mathbf{H}_{\mathbf{k}} = m\beta + \boldsymbol{\alpha} \cdot \mathbf{k}$ . The solution to (4.4) is given by  $\tilde{\psi}(t) = \exp(-it\mathbf{H}_{\mathbf{k}})\tilde{\psi}(0)$ , where

$$\exp(-it\mathbf{H}_{\mathbf{k}}) = \cos(\Omega t)I - (i/\Omega) \sin(\Omega t)\mathbf{H}_{\mathbf{k}}, \quad (4.5)$$

and  $\Omega = (m^2 + |\mathbf{k}|^2)^{1/2}$ . Exponentially accurate numerical solutions in periodic domains may be computed by expressing the initial  $\psi$  as a Fourier series, and evolving each Fourier coefficient using (4.5). Transformations between grid-point values and Fourier coefficients may be computed efficiently using fast Fourier transforms.

## 5. Particle in a harmonic potential

We consider the same initial conditions, with zero initial momentum, confined by a harmonic potential  $V(\mathbf{x}) = -\frac{1}{2}m\omega_0^2|\mathbf{x}|^2$  under our sign convention. Setting  $\omega_0 = 1/(2m\Delta_0^2)$  leads to the initial spread  $\Delta_0$  of the wavepacket being preserved by subsequent evolution under the Schrödinger equation. For this test case we consider a cube with side length  $\ell = 200$ , mass  $m = 0.1$  and initial spread  $\Delta_0 = 14$ . To avoid the convergence properties being affected by discontinuities in the gradient of  $V$  at periodic boundaries, we approximate  $|\mathbf{x}|^2$  by  $v(x) + v(y) + v(z)$ , where the function  $v(x)$  is the first 6 terms of a Fourier cosine series approximation to  $x^2$  in  $[-\ell, \ell]$ .

(a) *Reference solutions*

A spatially varying potential couples the different Fourier modes, so exact solutions cannot be computed as Fourier series. However, accurate approximations may

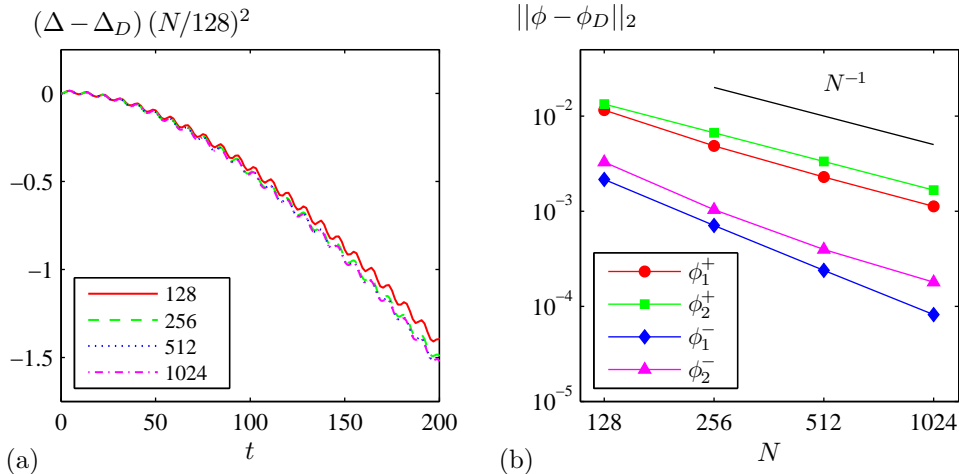


Figure 2. (Online version in colour.) (a) Second order convergence of the spreads  $\Delta$  towards the reference solution  $\Delta_D$  of the Dirac equation. (b) First order convergence of the moduli of the four fields  $\phi_{1,2}^\pm$  towards the reference solution  $\phi_{1,2}^\pm_D$  at  $t = 200$ .

be obtained by splitting the Hamiltonian. The free particle Hamiltonian  $H_{\mathbf{k}}$  decouples into one  $4 \times 4$  block for each Fourier mode, as above. The coupling Hamiltonian  $H_g = -g(\mathbf{x})I$  is diagonal in physical space, with a time-evolution operator given by

$$[\exp(-i\Delta t H_g)\psi](\mathbf{x}, t) = \exp(i\Delta t g(\mathbf{x}))\psi(\mathbf{x}, t). \quad (5.1)$$

Thus  $g$  is *minus* the dimensionless potential energy in our sign convention. Strang splitting approximates the coupled evolution to second order accuracy by using

$$\exp(-i\Delta t H) = \exp(-\frac{1}{2}i\Delta t H_g) \exp(-i\Delta t H_{\mathbf{k}}) \exp(-\frac{1}{2}i\Delta t H_g) + \mathcal{O}(\Delta t^3). \quad (5.2)$$

For the reference computations we used Forest & Ruth's (1990) fourth-order accurate splitting into seven steps, with an overall timestep  $\Delta t = 1.0$  and  $128^3$  Fourier modes. This solution was indistinguishable, for comparison purposes, from one computed with  $\Delta t = 0.25$  and  $256^3$  Fourier modes.

### (b) Results

Figure 3(a) shows the evolution of the spread  $\Delta$  for the reference solution, and for four QLB solutions on  $N^3$  grids with  $N = 128, 256, 512, 1024$ . All solutions are in good agreement for  $0 \leq t \lesssim 75$ , after which the initially regular oscillations are disrupted by negative energy states reflecting from the periodic boundaries. The solutions appear very sensitive to small errors due to the finite resolution, as shown by the diverging trajectories. Figure 3(b) shows similar behaviour in the squared  $L_2$  norms of the negative-energy components  $\phi_{1,2}^-$ , as normalised by  $M = \sum \|\phi_{1,2}^\pm\|^2$  and  $2M$  respectively. These two components are initially related by  $\|\phi_2^-\|^2 = 2\|\phi_1^-\|^2$ , as expected for solutions in which  $\phi_1^+$  is spherically symmetric and  $\|\phi_2^+\| \ll \|\phi_1^+\|$ . Again, the numerical solutions diverge away from this relation when  $t \approx 100$ . However, at  $t = 100$  we still have first-order convergence of all four components  $\phi_{1,2}^\pm$  of the QLB solutions towards the reference solution, as shown in

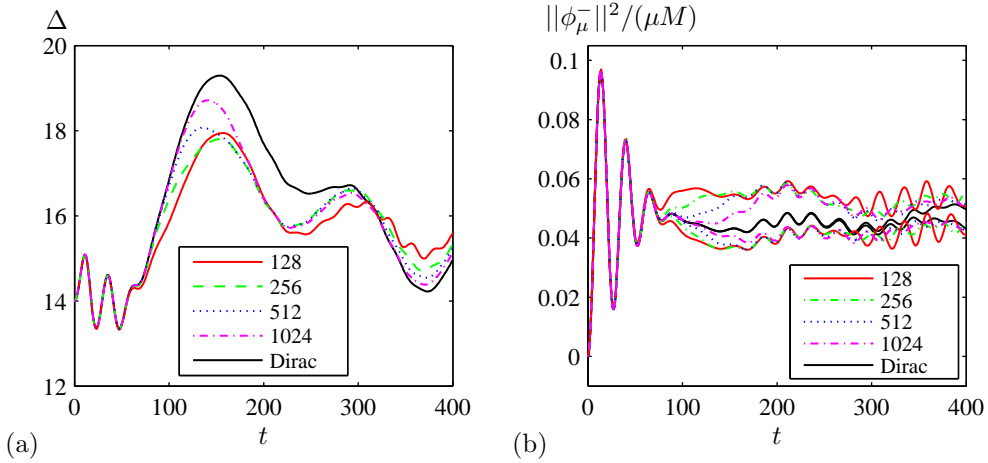


Figure 3. (Online version in colour.) Evolution of the (a) the spread  $\Delta$ , and (b) the relative magnitudes  $\|\phi_\mu^-\|^2/(\mu M)$  of the negative-energy components, for different grid resolutions.

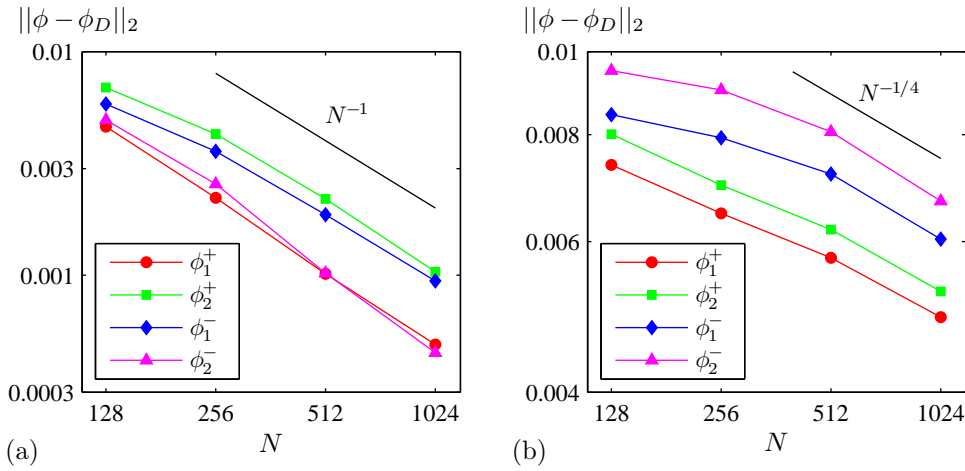


Figure 4. (Online version in colour.) Convergence of the four components  $\phi_{1,2}^\pm$  towards the reference solutions at (a)  $t = 100$  and (b)  $t = 400$  as the number of gridpoints  $N$  increases.

figure 4(a). The rate of convergence deteriorates at later times, due to the apparent sensitivity of the solution for  $t \approx 100$ . The measured convergence rate at  $t = 400$  is only  $N^{-1/4}$  over the range of resolutions used, as shown in figure 4(b).

## 6. Conclusion

The quantum lattice Boltzmann schemes are viable numerical schemes for solving the Dirac equation, not just for recovering its non-relativistic limit. Each step within the schemes is unitary, and at least second order accurate. However, the overall schemes are only first order accurate due to operator splitting. We presented numerical evidence of first order convergence towards highly accurate reference solutions for all four components of the Dirac wavefunction. The oscillations seen

in the numerical output of QLB schemes that are not present in the Schrödinger equation are explained as relativistic effects due to the finite mass of the particle.

We thank Silvia Palpacelli and Sauro Succi for useful conversations. P.J.D.'s research is supported by an EPSRC Advanced Research Fellowship, grant number EP/E054625/1. D.L. is supported by an attached project studentship. The computations made use of the FFTW3 library (Frigo & Johnson, 2005) and the Oxford Supercomputing Centre facilities.

## References

- Benzi, R., Succi, S. & Vergassola, M. 1992 The lattice Boltzmann equation: theory and applications. *Phys. Rept.*, **222**, 145–197.
- Berestetskii, V. B., Pitaevskii, L. P. & Lifshitz, E. 1982 *Quantum electrodynamics*. Butterworth–Heinemann, 2nd edn.
- Bialynicki-Birula, I. 1994 Weyl, Dirac, and Maxwell equations on a lattice as unitary cellular automata. *Phys. Rev. D*, **49**, 6920–6927.
- Chen, S. & Doolen, G. D. 1998 Lattice Boltzmann method for fluid flows. *Annu. Rev. Fluid Mech.*, **30**, 329–364.
- Dellar, P. J., Lapitski, D., Palpacelli, S. & Succi, S. 2010 A note on the isotropy of three-dimensional quantum lattice Boltzmann schemes. *Phys. Rev E*, submitted.
- Forest, E. & Ruth, R. D. 1990 Fourth-order symplectic integration. *Physica D*, **43**, 105–117.
- Frigo, M. & Johnson, S. G. 2005 The design and implementation of FFTW3. *Proc. IEEE*, **93**, 216–231.
- He, X., Chen, S. & Doolen, G. D. 1998 A novel thermal model of the lattice Boltzmann method in incompressible limit. *J. Comput. Phys.*, **146**, 282–300.
- Meyer, D. A. 1996 From quantum cellular automata to quantum lattice gases. *J. Statist. Phys.*, **85**, 551–574.
- Palpacelli, S. & Succi, S. 2007 Numerical validation of the quantum lattice Boltzmann scheme in two and three dimensions. *Phys. Rev. E*, **75**, 066 704–13.
- Palpacelli, S. & Succi, S. 2008 The quantum lattice Boltzmann equation: Recent developments. *Commun. Comput. Phys.*, **4**, 980–1007.
- Succi, S. 1996 Numerical solution of the Schrödinger equation using discrete kinetic theory. *Phys. Rev. E*, **53**, 1969–1975.
- Succi, S. 2001 *The lattice Boltzmann equation: For fluid dynamics and beyond*. Oxford: Oxford University Press.
- Succi, S. & Benzi, R. 1993 Lattice Boltzmann equation for quantum mechanics. *Physica D*, **69**, 327–332.
- Valdivieso, M. A. & Muñoz, J. D. 2009 Numerical comparison of 1D quantum lattice Boltzmann models. *J. Statist. Mech.: Theory & Expt*, P06 004–8.
- Whitham, G. B. 1974 *Linear and nonlinear waves*. New York: Wiley Interscience.